Letter

Universal superdiffusion of random walks in media with embedded fractal networks of low diffusivity

Fábio D. A. Aarão Reis [*]
Instituto de Física, Universidade Federal Fluminense, Avenida Litorânea s/n, 24210-340 Niterói, Rio de Janeiro, Brazil

Vaughan R. Voller [†]
Department of Civil, Environmental, and Geo- Engineering and Saint Anthony Falls Laboratory, University of Minnesota, 500 Pillsbury Drive SE, Minneapolis, Minnesota 55455, USA

(Received 25 February 2024; revised 3 June 2024; accepted 28 June 2024; published 1 August 2024)

Diffusion in composite media with high contrasts between diffusion coefficients in fractal sets of inclusions and in their embedding matrices is modeled by lattice random walks (RWs) with probabilities $p < 1$ of hops from fractal sites and 1 from matrix sites. Superdiffusion is predicted in time intervals that depend on p and with diffusion exponents that depend on the dimensions of matrix (E) and fractal (D_F) as $\nu = 1/(2 + D_F - E)$. This contrasts with the nonuniversal subdiffusion of RWs confined to fractal media. Simulations with four fractals show the anomaly at several time decades for $p \lesssim 10^{-3}$ and the crossover to the asymptotic normal diffusion. These results show that superdiffusion can be observed in isotropic RWs with finite moments of hop length distributions and allow the estimation of the dimension of the inclusion set from the diffusion exponent. However, displacements within single trajectories have normal scaling, which shows transient ergodicity breaking.

DOI: 10.1103/PhysRevE.110.L022102

Diffusion in porous media has applications in heterogeneous catalysis, membrane separation, environmental remediation, and rock weathering [1–4]. In homogeneous media, the mean square displacement (MSD) of diffusing tracers or diffusing fronts linearly increase with time t as $\langle r^2 \rangle = 2Dt$, where D is the diffusion coefficient. In materials with the same chemical properties but different morphologies, the values of D for a given tracer may vary three orders of magnitude or more; for instance, chloride diffusion coefficients in compacted bentonite vary from $\sim 10^{-10}$ m^2/s to $\sim 10^{-13}$ m^2/s for porosity from ∼30% to ∼0.3% [5], iodide coefficients in limestones with the same range for porosity vary from ∼3% to ∼40% [6], and U(VI) coefficients from $\sim 10^{-15}$ m^2/s to 10^{-12} m^2/s are measured in bentonite with porosity between ∼0.02% and ∼7% [7]. In materials with different chemical compositions, the values of D may differ by much more than three orders; the time evolutions of the MSD in two homogeneous media with such high contrasts in diffusivities are schematically illustrated by the top and bottom dashed lines in Fig. 1. In a composite where small domains of one of these materials are periodically or randomly distributed within the other material, the diffusion coefficient is averaged over the concentrations of those components, following the intermediate dashed line in Fig. 1.

However, correlations in the heterogeneity distributions are frequent in natural and manufactured media; for instance, a fractal organization may result from the aggregation dynamics of a heterogeneous medium [8,9]. This may result in anomalous behavior of the MSD as

$$\langle r^2 \rangle \sim t^{2\nu} \tag{1}$$

with $\nu \neq 1/2$ [10–13]. If the diffusion is restricted to the fractal component (e.g., impermeable solid with fractal pore network), several studies showed subdiffusion ($\nu < 1/2$) because the diffusing tracers or fronts encounter self-similar distributions of obstacles as they advance [14,15]. This is illustrated by the dotted line in Fig. 1 for a fractal medium formed by the low conductivity material. The exponent ν is nonuniversal because it is not solely a function of the fractal dimension D_F of that medium. For instance, the exact values of ν in a Sierpinski gasket [14] and in a T-fractal [16] with exactly the same D_F are different, while simulations show very different values of ν (≈0.47, ≈0.35) in Sierpinski carpets [17] and percolation clusters [18] with nearly the same D_F; see Ref. [19].

Superdiffusion ($\nu > 1/2$) is also observed in several processes, such as those whose jump size distributions have long tails (e.g., Lévy walks and flights) [12,20,21], sediment transport [22,23], phase change problems [24], fluid infiltration [25–27], contaminant transport in aquifiers [28,29], continuous time random walks (RWs) with correlated jump lengths [10,11], diffusion with extended temporal correlations [30–32] or with memory [33,34], and other nonlinear diffusion processes [35]. Driven motion in disordered media may also lead to superdiffusion in several time decades before the crossovers to normal behavior [36–39]. However, to our knowledge, all previous models of isotropic RWs with finite moments of hop length distributions exhibited normal or subdiffusive scaling in disordered media (dashed and dotted

[*]Contact author: fdaar@protonmail.com
[†]Contact author: volle001@umn.edu

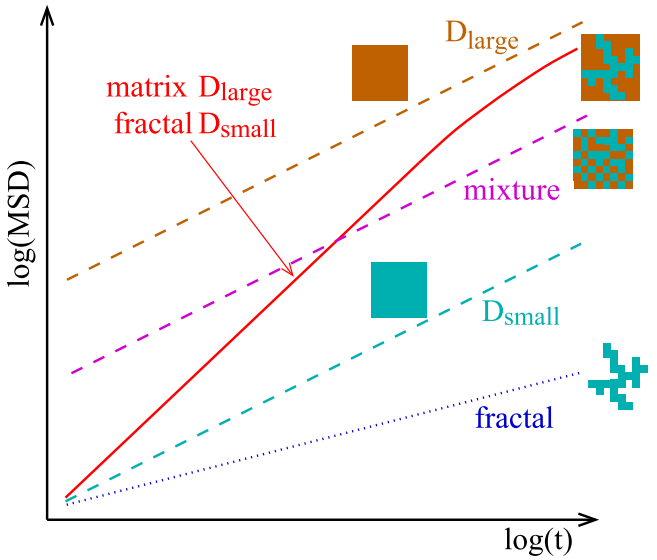

FIG. 1. Time evolution of the MSD in homogeneous and composite media whose geometries are schematically illustrated. The diffusion coefficient is much larger in the brown (darkest gray) material than in the cyan (lightest gray) material and dashed lines with slope 1 correspond to normal diffusion.

lines in Fig. 1) because the disorder retards the walker spreading.

In this Letter, we study diffusion in composite media with a two- or three-dimensional matrix and an embedded fractal network of inclusions where the diffusion coefficient is smaller than that of the matrix. If the diffusing species is injected at the fractal network, we will show that the MSD scaling is qualitatively represented by the solid line in Fig. 1. This is a superdiffusive behavior ($\nu > 1/2$) in a number of time decades that increases as the diffusivity contrast between the two components increases. This result is obtained in a RW model on lattices whose sites represent small domains of each component and in which different hop probabilities represent the different diffusion coefficients in those components. Compared to other models, superdiffusion is observed here with much simpler physical mechanisms: hop length distributions are finite, the motion is not driven, and there is no memory effect. Moreover, contrary to subdiffusive systems, the superdiffusion is universal because the exponent ν depends only on the dimensions of the inclusion set and of the embedding matrix.

The RW model is defined in a hypercubic lattice of dimension E where a fractal with dimension D_F is embedded. We refer to the fractal sites as inclusions and to the remaining sites as matrix. Each site represents a nanoscopic or microscopic homogeneous domain with one of the two components. The edge length a of a site is the maximal length scale of the composite with homogeneous properties. A tracer is left at a randomly chosen inclusion at $t = 0$ and attempts to hop to a randomly chosen nearest neighbor (NN) site in each time interval s. If the tracer is at the matrix, the hop is executed with probability 1; if it is at an inclusion, the hop is executed with probability p, otherwise it remains in the same position; see Fig. 2(a). Thus, s and s/p are the average residence times

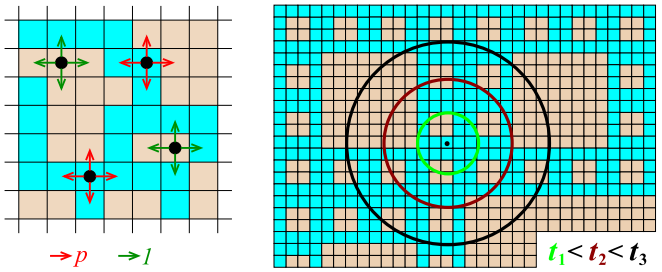

FIG. 2. (a) Possible hops (arrows) of tracers (black dots) at matrix sites (brown or darkest gray) and at inclusions (cyan or lightest gray), with the corresponding probabilities of executing the hops. (b) Circles centered at the initial position (small black dot) approximate the regions scanned by a tracer at three times. The inclusions form a Sierpinski carpet pattern.

of the tracer in matrix and inclusion sites, respectively. In a composite, p is the contrast of diffusion coefficients of matrix and inclusions, so $p \ll 1$ is a realistic possibility.

The splitting of a porous medium into two regions with different transport properties (e.g., diffusion coefficient or hydraulic conductivity) is equivalent to the double (or dual) porosity modeling of flow in geological formations [40]. Our model may find applications to naturally fractured reservoirs of type IV, in which minerals form barriers to fluid or solute transport in fractures [41]. Moreover, the limit $p \to 0$ of our model is similar to the recently proposed butterfly diffusion model [42].

Since the hop directions are randomly chosen at each site, the tracer spreads as in a RW in dimension E. As the time increases, the tracer scans wider regions centered at the starting point; see Fig. 2(b). The fraction of visited inclusion sites decreases with the observation radius r as [8,9]

$$\rho \sim r^{-\Delta}, \quad \Delta = E - D_F. \tag{2}$$

At short times the tracer is frequently stuck at the inclusions [e.g., t_1 in Fig. 2(b)], but as the time increases it crosses an increasing fraction of matrix sites [e.g., large brown areas inside the circle at t_3 in Fig. 2(b)]. This leads to faster spread as time increases and qualitatively explains the superdiffusion. However, Eq. (2) is applicable only if the origin is a point of the fractal and if the fractal does not have disconnected parts.

Now we determine the ensemble average MSD, abreviately denoted as r^2, partly following scaling approaches previously applied to infiltration problems [43,44].

Let $N \gg 1$ be the number of executed hops at time t, so that $N + 1 \approx N$ sites were visited by the tracer. Letting N_F be the number of visited sites of the fractal (inclusions) and remembering that the tracers are uniformly spread in a radius $\sim r$, the fraction of visited sites belonging to the fractal scales as the density in Eq. (2):

$$\frac{N_F}{N} \approx C\left(\frac{r}{a}\right)^{-\Delta}, \tag{3}$$

where $C \sim 1$ is a dimensionless constant. The number of hops executed from matrix sites is $N - N_F$. The time t is then split into average hopping times in each set, which are obtained from the numbers of executed hops and the average

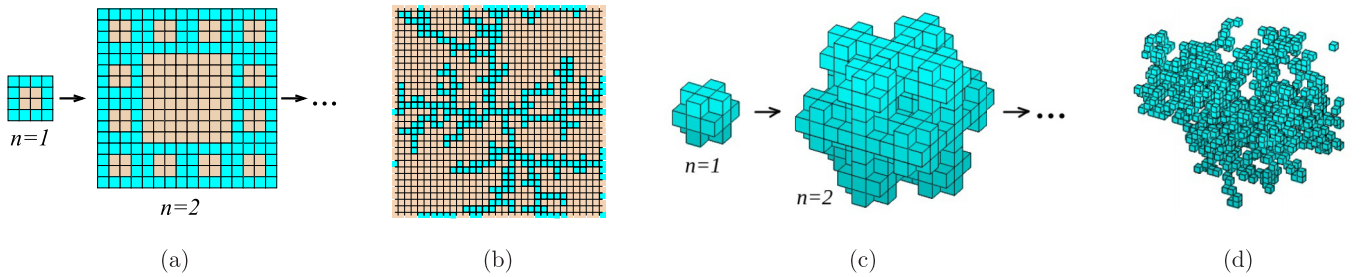

FIG. 3. Media in which simulations are performed, with inclusion sites in cyan (lightest gray) and matrix sites [shown only in the two-dimensional (2D) media] in brown (darkest gray). (a) First two stages of construction of a Sierpinski carpet ($D_F = \ln 12/\ln 4 \approx 1.7924$). (b) Central region of a DLA ($D_F \approx 1.71$) [8]. (c) First two stages of construction of a generalized Menger sponge ($D_F = \ln 19/\ln 3 \approx 2.6801$). (d) Central region of critical percolation cluster in simple cubic lattice with NN and next NN connectivity ($D_F \approx 2.53$) [46].

residence times:

$$t = N_F \frac{s}{p} + (N - N_F)s. \tag{4}$$

For $p \ll 1$, the number of hop attempts t/s may be much larger than N.

The uniform spread of tracers that executed N hops imply

$$r^2 = Na^2. \tag{5}$$

Eqs. (3), (4), and (5) then give

$$\left(\frac{r}{a}\right)^2 \approx \frac{t}{s}\left[1 + C\left(\frac{1}{p} - 1\right)\left(\frac{r}{a}\right)^{-\Delta}\right]^{-1}. \tag{6}$$

For $p \ll 1$ and r not too large, the second term inside the brackets is dominant, which leads to

$$r \approx a\left(\frac{p}{C}\frac{t}{s}\right)^{\nu}, \quad \nu = \frac{1}{2 - \Delta}, \tag{7}$$

where Δ is in Eq. (2). We typically expect that $0 < \Delta < 1$, e.g., for a fractal with $D_F > 2$ embedded in a 3D matrix. Equation (7) predicts universal superdiffusive behavior in which $1/2 < \nu < 1$ and ν depends only on D_F and E. This is in striking contrast with the nonuniversal exponents of subdiffusion confined to fractal media [14,19].

We performed simulations of the model with two fractals embedded in $E = 2$ and two fractals embedded in $E = 3$: Sierpinski carpet with scaling factor 4 and 2×2 blocks removed at each iteration, with removed blocks forming the matrix [$D_F = \ln 12/\ln 4 \approx 1.7924$; Fig. 3(a)]; diffusion limited aggregate (DLA) in a square lattice [$D_F \approx 1.71$ [8]; Fig. 3(b)]; generalized Menger sponge with scaling factor 3 and eight cubes removed from the vertices at each iteration, with removed cubes forming the matrix [$D_F = \ln 19/\ln 3 \approx 2.6801$; Fig. 3(c) with matrix sites not shown]; a critical percolation cluster in a simple cubic lattice with NN and next NN connectivity, with occupation probability 0.137 304 5(5) [45] and the remaining sites forming the matrix ($D_F \approx 2.53$ [46]) [Fig. 3(d) with matrix sites not shown]. Percolation clusters and DLAs represent several materials with fractal geometry [14,47], while laboratory made materials were already built with the geometry of deterministic fractals [48–50]. Simulation cells have lateral sizes $\sim 1.6\times10^4$ in $E = 2$ and ~ 700 in $E = 3$ (in units of a), while p ranged from 10^{-4} to 10^{-1}. The control of the simulation time ensures that no tracer reaches the borders of the simulation cells. Numerical results are presented with $a = 1$ and hop attempt time $s = 1$.

Figure 4 shows the evolution of $\langle r^2\rangle/t$ in those media and several values of p. This ratio increases in 1–3 time decades, which indicates superdiffusive behavior. Linear fits in those regions have the slopes shown in Fig. 4, which give $\nu = 0.55$ (carpet), 0.55 (DLA), 0.56 (sponge), and 0.64 (percolation cluster). Equation (7) with the known values of D_F give the respective values $\nu = 0.56$, 0.59, 0.60, and 0.65, which differ from simulation values by 2%–7%.

In $E = 1$, Eq. (7) gives the same exponent ν of fluid infiltration in layered media with low conductivity inclusions distributed as in Cantor sets [51]. Calculations for hydraulic conductivity contrasts $\gtrsim 50$ (easily found in geological materials [52]) showed that superdiffusive infiltration might be observed in realistic settings. The scaling behaviors of that model and of infiltration of diffusing tracers was shown to be the same [44], so the present model may be extended to fluid flow in materials with high contrasts in the hydraulic conductivities of the components. This may be relevant to explain

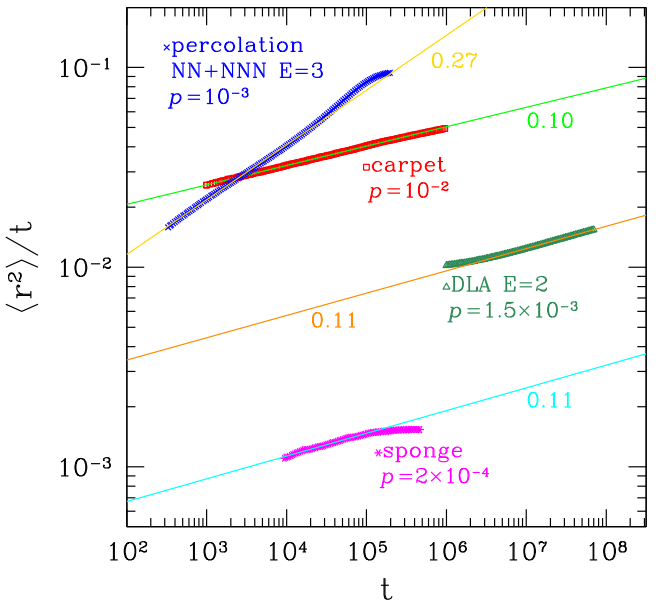

FIG. 4. Ratio between MSD and time in media with four inclusion patterns, with corresponding values of p and slopes of linear fits (straight lines).

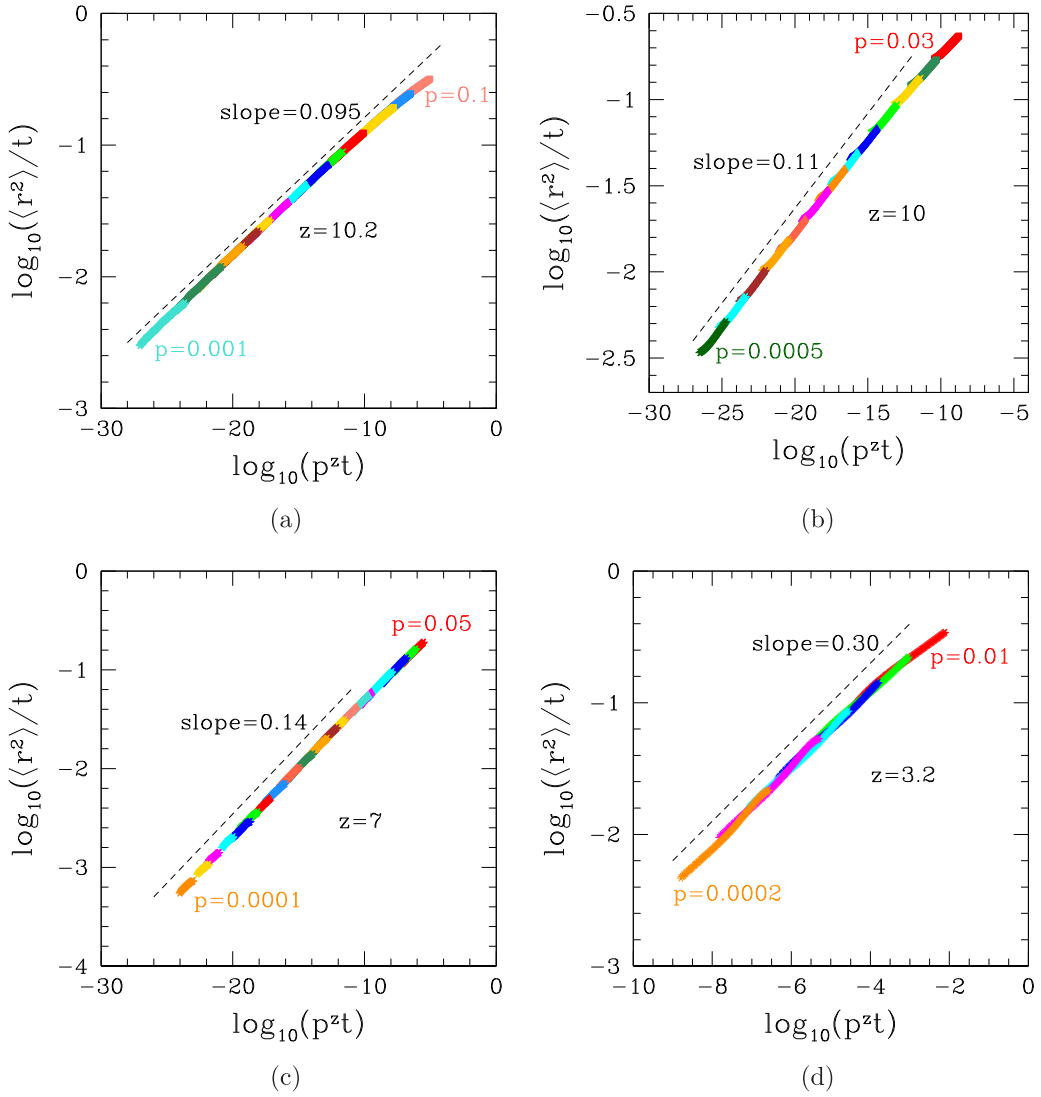

FIG. 5. Scaling plots following Eq. (10) with values of z indicated in each panel and inclusion patterns of (a) Sierpinski carpet, (b) DLA, (c) generalized Menger sponge, (d) critical percolation cluster. Minimal and maximal values of p are shown in each plot. Intermediate values of p vary by consecutive factors 1.25–1.5.

superdiffusive behavior of moisture infiltration in building materials [25,26,53], where there is no evidence of the usual mechanisms of superdiffusion (long distance hops, driven motion, or memory effects).

At sufficiently long times, the RW model crosses over to normal diffusion. This is clearly shown in Fig. 4 for 3D media due to the small simulation cells. The crossover occurs when the second term inside the brackets of Eq. (6) is of the same order as the first term; for $p \ll 1$, this occurs for $(r/a)^{\Delta} \sim C/p$. This condition and Eq. (7) predict a crossover time

$$t_c \sim s\left(\frac{p}{C}\right)^{-z}, \quad z = \frac{2}{\Delta}. \tag{8}$$

As expected, t_c increases as p decreases. The crossover exponent z is very large for small Δ (D_F close to E), which implies high sensitivity of the crossover time on variations of p and the possibility to observe superdiffusion in several time decades in systems with high contrasts in the diffusion coefficients. For the fractals considered in our simulations, z ranges from 4.3 to 9.6.

A dynamic scaling relation that fits anomalous and normal regimes can be written as

$$\left(\frac{r}{a}\right)^2 = \frac{t}{s}F\left(\frac{t}{t_c}\right), \tag{9}$$

where F has asymptotic forms $F(x) \sim x^{2\nu-1}$ for $x \ll 1$ and $F(x) \to 1$ for $x \gg 1$. In simulations with $a = 1$ and $s = 1$ we expect

$$\frac{\langle r^2\rangle}{t} = G(p^z t), \tag{10}$$

where G is a function with properties similar to F. Following this reasoning, Figs. 5(a)–5(d) show $\langle r^2\rangle/t$ as a function of $p^z t$ for the four fractal patterns. The values of z were chosen to provide the best data collapses (after removing short and long time data for each p). For the smallest p (left sides of the plots), the data collapse in a time increasing line shows that

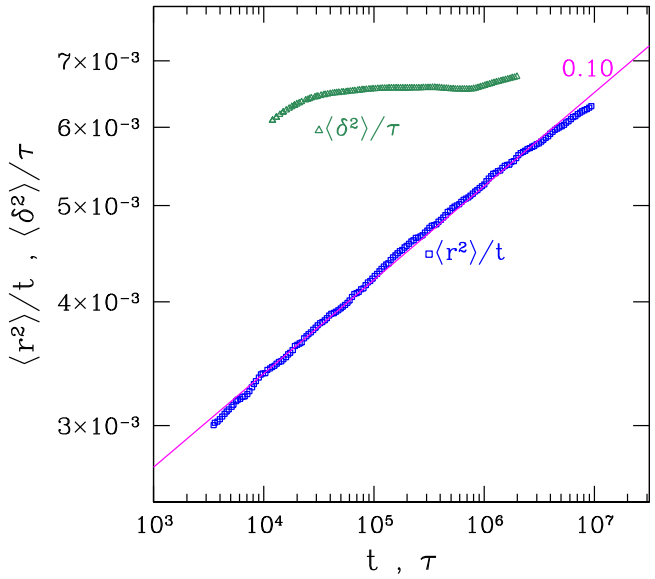

FIG. 6. Scaled ensemble and time averaged MSDs in the Sierpinski carpet. The linear fit (straight line) of the ensemble MSD has the indicated slope.

superdiffusion would be observed in a large number of time decades (5–15 decades) if much longer simulations were possible; of course, these longer simulations would require much larger lattices to avoid the finite-size effects. The smallest p in Figs. 5(a)–5(d) are of orders 10^{-4}–10^{-3}, which are diffusivity contrasts not difficult to find in natural or manufactured materials, so the expectation of superdiffusion is realistic in media whose geometries follow the present conditions.

From the numerical estimates of z, Eqs. (2) and (8) may be used to estimate D_F. The differences from the exact dimensions of regular fractals are from 0.6% to 1.8% and the differences from the numerically estimated dimensions of stochastic fractals are from 5% to 6%. However, deviations between the numerical and the theoretical values of z are larger, specially in the stochastic fractals; the theoretical values are 9.6 (carpet), 6.9 (DLA), 6.3 (sponge), and 4.3 (percolation cluster), to be compared with those in Figs. 5(a)–5(d). This occurs because small variations in D_F lead to large variations in Δ and, consequently, to large variations in z. Possible reasons for those deviations are that (i) the values in the stochastic fractals were obtained from large scale simulations instead of the relatively small lattices used here and (ii) the simulations are performed near the central regions of the fractal patterns, where the scalings of mass with observation radius may have corrections relatively to the asymptotic relations.

Now we analyze the scaling of the time averaged MSD $\langle\overline{\delta^2(\tau)}\rangle$, which represents a single tracer displacement in a time interval τ. It is calculated at two steps [54]: (i) the time averaged MSD over a trajectory with maximal time T is

$$\overline{\delta^2(\tau)} = \frac{1}{T-\tau}\int_0^{T-\tau} [\vec{x}(t+\tau)-\vec{x}(t)]^2 dt; \qquad (11)$$

(ii) $\overline{\delta^2(\tau)}$ is averaged over different trajectories (and different configurations in stochastic fractals). Figure 6 compares $\langle\overline{\delta^2(\tau)}\rangle/\tau$ in the Sierpinski carpet with the ensemble average $\langle r^2\rangle/t$. $\langle\overline{\delta^2(\tau)}\rangle/\tau$ has small variation in more than two time decades, which contrasts with the increase in $\langle r^2\rangle/t$; the oscillations of $\langle\overline{\delta^2(\tau)}\rangle/\tau$ are expected in RWs in deterministic fractals [55]. Thus, the model has a transient nonergodic behavior which may persist for very long times while the superdiffusive behavior of the ensemble average remains. Transient nonergodic behavior was also observed, e.g., in previous work on fractional Brownian motion driven by long-range correlated noise [56].

In order to explain this result, we recall that the density of a fractal set decreases with the radius where its mass is measured [Eq. (2)] only if the center of the observation windows is at the fractal. Instead, if the observation window has a center at the matrix, the density of inclusions may not follow Eq. (2) and may even be zero. For instance, if the center is in the middle of the largest hole of the Sierpinski carpet [Fig. 3(a)], fractal points will be found only in windows with radii of the same order of the lateral size of that hole. In such cases, the MSD will have normal scaling because the walker moves in the matrix almost all the time. A similar situation occurs when the time averaged MSD is measured [Eq. (11)]: the starting point of this measurement may be in the matrix or in the fractal, but, as the trajectory time increases, the probability of a starting point in the matrix increases. Thus, for sufficiently long trajectories [large T in Eq. (11)], normal scaling of $\langle\overline{\delta^2(\tau)}\rangle$ is expected for $\tau \ll T$.

Finally, our RW model in $E = 1$ can be related to a continuous model with the diffusion coefficient varying as a power law of the position x: $D(x) \sim x^\alpha$ with $\alpha > 0$ [54,57]. In the RW model, consider a coarse-grained region of width w (w/a sites) around position x and with $a \ll w \ll x$. Inside this region, the fraction of sites with inclusions is $f \approx C(x/a)^{-\Delta}$ with $C \sim 1$ [Eq. (2)], whereas the remaining sites (fraction $1-f$) are matrix sites. Diffusion coefficients D_0 and pD_0 are associated to matrix and inclusion sites, respectively. Considering the association in series of the diffusion coefficients in that region, the equivalent diffusion coefficient is

$$D(x) \approx \left[f\left(\frac{w}{a}\right)\frac{1}{pD_0} + (1-f)\left(\frac{w}{a}\right)\frac{1}{D_0}\right]^{-1}. \qquad (12)$$

For $p \ll 1$, the first term inside the brackets is dominant and, using the above form for f, we obtain

$$D(x) \approx \frac{apD_0}{wC}(x/a)^\Delta. \qquad (13)$$

This gives $\alpha = \Delta$ in the framework of Cherstvy *et al.* [54,57], who showed that ν obeys Eq. (7) with α replacing Δ. Notably, that work also showed ergodicity breaking. The above arguments may be extended to $E = 3$, in which Hernandez-Coronado *et al.* [58] showed superdiffusion in an advective-dispersive equation when the diffusion coefficient increases with the distance from the origin [with an exponent also consistent with Eq. (7)].

In summary, we introduced a model for tracer diffusion in composite materials where fractal networks of inclusions with low diffusivity are embedded in 2D or 3D matrices with high diffusivity. To comply with these conditions, we proposed a simple RW model on lattices in which the hopping rate from inclusion sites is much smaller than the hopping

rate from matrix sites and stuck to cases where the diffusing tracers are released at the inclusions. A scaling approach predicted superdiffusion (RW exponent $>1/2$) in a number of time decades that increases with the diffusivity contrast and predicted the crossover to asymptotically normal diffusion. The superdiffusion exponent is universal because it depends only on the dimensions of the fractal and of the matrix. To our knowledge, such a result was not formerly obtained in isotropic lattice RWs with hops to neighboring sites. The result is in striking contrast with the nonuniversal subdiffusion of RWs whose motion is restricted to a fractal network embedded in an impermeable solid. Numerical simulations with regular and stochastic fractals embedded in 2D and 3D matrices confirmed the superdiffusion and the predicted exponents with accuracy better than 10%. The numerical test of a dynamic scaling relation shows that the diffusion anomaly may appear in 5 to 15 time decades for diffusivity contrasts between 10^{-4} and 10^{-3}. Depending on the choice of porous materials to form a composite, tracer diffusion coefficients may actually differ by two or more orders of magnitude [2,4], so it is plausible that superdiffusion in this type of heterogeneous media can be observed. However, these results are applicable to ensemble averages only, while the time averaged MSD in a single trajectory has normal behavior because its calculation considers most starting points in the matrix.

F.D.A.A.R. acknowledges support by the Brazilian agencies CNPq (305391/2018-6), FAPERJ (E-26/210.040/2020, E-26/201.050/2022), and CAPES (88887.310427/2018-00). V.R.V. acknowledges support from the James L. Record Professorship.

[1] P. M. Adler, *Porous Media: Geometry and Transports* (Butterworth-Heinemann, Stoneham, MA, 1992).
[2] P. Grathwohl, *Diffusion in Natural Porous Media: Contaminant Transport, Sorption/Desorption and Dissolution Kinetics* (Springer, New York, 1998).
[3] B. Coasne, New J. Chem. **40**, 4078 (2016).
[4] B. C. Bukowski, F. J. Keil, P. I. Ravikovitch, G. Sastre, R. Q. Snurr, and M. Coppens, Adsorption **27**, 683 (2021).
[5] L. R. V. Loon, M. A. Glaus, and W. Muller, Appl. Geochem. **22**, 2536 (2007).
[6] T. B. Boving and P. Grathwohl, J. Contam. Hydrol. **53**, 85 (2001).
[7] C. Joseph, J. Mibus, P. Trepte, C. Muller, V. Brendler, D. M. Park, Y. Jiao, A. B. Kersting, and M. Zavarin, Sci. Total Environ. **575**, 207 (2017).
[8] T. Vicsek, *Fractal Growth Phenomena*, 2nd ed. (World Scientific, Singapore, 1991).
[9] M. Elimelech, J. Gregory, X. Jia, and R. A. Williams, *Particle Deposition and Aggregation: Measurement, Modelling and Simulation* (Butterworth-Heinemann, Woburn, MA, 1995).
[10] J. P. Bouchaud and A. Georges, Phys. Rep. **195**, 127 (1990).
[11] R. Metzler and J. Klafter, Phys. Rep. **339**, 1 (2000).
[12] R. Metzler, J.-H. Jeon, A. G. Cherstvy, and E. Barkai, Phys. Chem. Chem. Phys. **16**, 24128 (2014).
[13] F. A. Oliveira, R. M. S. Ferreira, L. C. Lapas, and M. H. Vainstein, Front. Phys. **7**, 18 (2019).
[14] S. Havlin and D. Ben-Avraham, Adv. Phys. **51**, 187 (2002).
[15] A. S. Balankin, J. Ramírez-Joachin, G. González-López, and S. Gutíerrez-Hernández, Chaos Solitons Fractals **162**, 112452 (2022).
[16] A. Giacometti, A. Maritan, and H. Nakanishi, J. Stat. Phys. **75**, 669 (1994).
[17] A. Balankin, Phys. Lett. A **381**, 2801 (2017).
[18] P. Grassberger, Physica A **262**, 251 (1999).
[19] F. D. A. A. Reis, J. Phys. A: Math. Gen. **29**, 7803 (1996).
[20] G. M. Viswanathan, E. P. Raposo, and M. G. E. da Luz, Phys. Life Rev. **5**, 133 (2008).
[21] A. K. Golmankhaneh and A. S. Balankin, Phys. Lett. A **382**, 960 (2018).
[22] Z. Wu, E. Foufoula-Georgiou, G. Parker, A. Singh, X. Fu, and G. Wang, J. Geophys. Res: Earth Surface **124**, 21 (2019).
[23] K. L. G. Pretzlav, J. P. L. Johnson, and D. N. Bradley, Geophys. Res. Lett. **48**, e2020GL091991 (2021).
[24] V. R. Voller, Int. J. Numerical Methods Heat Fluid Flow **26**, 624 (2016).
[25] M. Küntz and P. Lavallée, J. Phys. D **34**, 2547 (2001).
[26] A. El Abd, Appl. Radiat. Isot. **105**, 150 (2015).
[27] F. D. A. A. Reis, D. Bolster, and V. R. Voller, Adv. Water Resour. **113**, 180 (2018).
[28] C. Zheng, M. Bianchi, and S. M. Gorelick, Ground Water **49**, 649 (2011).
[29] M. Yin, Y. Zhang, R. Ma, G. R. Tick, M. Bianchi, C. Zheng, W. Wei, S. Wei, and X. Liu, J. Hydrol. **582**, 124515 (2020).
[30] D. Molina-Garcia, T. Sandev, H. Safdari, G. Pagnini, A. Chechkin, and R. Metzler, New J. Phys. **20**, 103027 (2018).
[31] C. W. Tsai, S.-H. Huang, and S. Y. Hung, Water Resour. Res. **57**, e2020WR028475 (2021).
[32] S. Yui, Y. Tang, W. Guo, H. Kobayashi, and M. Tsubota, Phys. Rev. Lett. **129**, 025301 (2022).
[33] M. H. Vainstein, I. V. L. Costa, R. Morgado, and F. A. Oliveira, Europhys. Lett. **73**, 726 (2006).
[34] Z. Shen, F. Plouraboué, J. S. Lintuvuori, H. Zhang, M. Abbasi, and C. Misbah, Phys. Rev. Lett. **130**, 014001 (2023).
[35] L. C. Malacarne, R. S. Mendes, I. T. Pedron, and E. K. Lenzi, Phys. Rev. E **63**, 030101(R) (2001).
[36] D. Winter, J. Horbach, P. Virnau, and K. Binder, Phys. Rev. Lett. **108**, 028303 (2012).
[37] O. Bénichou, A. Bodrova, D. Chakraborty, P. Illien, A. Law, C. Mejía-Monasterio, G. Oshanin, and R. Voituriez, Phys. Rev. Lett. **111**, 260601 (2013).
[38] C. F. E. Schroer and A. Heuer, Phys. Rev. Lett. **110**, 067801 (2013).
[39] S. Leitmann and T. Franosch, Phys. Rev. Lett. **118**, 018001 (2017).
[40] J. E. Warren and P. J. Root, Soc. Petrol. Engs. J. **3**, 245 (1963).
[41] R. A. Nelson, *Geologic Analysis of Naturally Fractured Reservoirs* (Gulf Professional, Boston, 2001).
[42] F. Gaspar and J. Kukal, Physica A **646**, 129893 (2024).

[43] F. D. A. A. Reis, Phys. Rev. E **94**, 052124 (2016).
[44] F. D. A. A. Reis and V. R. Voller, Phys. Rev. E **99**, 042111 (2019).
[45] Z. Xun, D. Hao, and R. M. Ziff, Phys. Rev. E **105**, 024105 (2022).
[46] H. G. Ballesteros, L. A. Fernández, V. Martín-Mayor, A. M. Sudupe, G. Parisi, and J. J. Ruiz-Lorenzo, J. Phys. A: Math. Gen. **32**, 1 (1999).
[47] D. Stauffer and A. Aharony, *Introduction to Percolation Theory* (Taylor & Francis, London/Philadelphia, 1992).
[48] N. Filipovitch, K. Hill, A. Longjas, and V. Voller, Water Resour. Res. **52**, 5167 (2016).
[49] X.-Y. Xu, X.-W. Wang, D.-Y. Chen, C. M. Smith, and X.-M. Jin, Nat. Photon. **15**, 703 (2021).
[50] F. De Nicola, N. S. P. Purayil, D. Spirito, M. Miscuglio, F. Tantussi, A. Tomadin, F. De Angelis, M. Polini, R. Krahne, and V. Pellegrini, ACS Photon. **5**, 2418 (2018).
[51] V. R. Voller and F. D. A. A. Reis, Adv. Water Resour. **172**, 104365 (2023).
[52] O. D. L. Strack, *Groundwater Mechanics* (Prentice-Hall, Englewood Cliffs, NJ, 1989).
[53] A. E. G. El-Abd and J. J. Milczarek, J. Phys. D: Appl. Phys. **37**, 2305 (2004).
[54] A. G. Cherstvy, A. V. Chechkin, and R. Metzler, New J. Phys. **15**, 083039 (2013).
[55] M. A. Bab, G. Fabricius, and E. V. Albano, J. Chem. Phys. **128**, 044911 (2008).
[56] W. Deng and E. Barkai, Phys. Rev. E **79**, 011112 (2009).
[57] A. G. Cherstvy and R. Metzler, Phys. Rev. E **90**, 012134 (2014).
[58] H. Hernandez-Coronado, M. Coronado, and E. C. Herrera-Hernandez, Phys. Rev. E **85**, 066316 (2012).